

Texas Spectroscopic Search for Ly α Emission at the End of Reionization II. The Deepest Near-Infrared Spectroscopic Observation at $z \gtrsim 7$

INTAE JUNG,¹ STEVEN L. FINKELSTEIN,¹ MARK DICKINSON,² TAYLOR A. HUTCHISON,^{3,4} REBECCA L. LARSON,¹
CASEY PAPOVICH,^{3,4} LAURA PENTERICCI,⁵ MIMI SONG,⁶ HENRY C. FERGUSON,⁷ YICHENG GUO,⁸ SANGEETA MALHOTRA,^{6,9}
BAHRAM MOBASHER,¹⁰ JAMES RHOADS,^{6,9} VITHAL TILVI,⁹ AND ISAK WOLD⁶

¹*Department of Astronomy, The University of Texas at Austin, Austin, TX 78712, USA*

²*National Optical Astronomy Observatory, Tucson, AZ 85719, USA*

³*Department of Physics and Astronomy, Texas A&M University, College Station, TX, 77843-4242 USA*

⁴*George P. and Cynthia Woods Mitchell Institute for Fundamental Physics and Astronomy, Texas A&M University, College Station, TX, 77843-4242 USA*

⁵*INAF, Osservatorio Astronomico di Roma, via Frascati 33, 00078, Monteporzio Catone, Italy*

⁶*Astrophysics Science Division, Goddard Space Flight Center, Greenbelt, MD 20771, USA*

⁷*Space Telescope Science Institute, 3700 San Martin Drive, Baltimore, MD 21218, USA*

⁸*Department of Physics and Astronomy, University of Missouri, Columbia, MO, USA*

⁹*School of Earth & Space Exploration, Arizona State University, Tempe, AZ 85287, USA*

¹⁰*Department of Physics and Astronomy, University of California, Riverside, CA 92521, USA*

Submitted to *the Astrophysical Journal*

ABSTRACT

Realizing the utility of Ly α emission to trace the evolution of the intergalactic medium (IGM) during the epoch of reionization requires deep spectroscopy across the boundary of optical and near-infrared (NIR) spectrographs at $z \sim 7.2$ when Ly α emission is at $\sim 1\mu\text{m}$. Our Texas Spectroscopic Search for Ly α Emission at the End of Reionization includes 18 nights of deep spectroscopic observations using the Keck DEIMOS (optical) and MOSFIRE (NIR) spectrographs. Within this dataset we observe Ly α emission from 183 photometric-redshift selected galaxies at $z = 5.5 - 8.3$ from the Cosmic Assembly Near infrared Deep Extragalactic Legacy Survey (CANDELS). Our overlapping MOSFIRE observations, over 84 galaxies total, provide the deepest NIR spectroscopic data yet obtained for Ly α from galaxies $z > 7$, with > 16 hr integration time for *four* observed galaxies. Here we analyze these four targets, and we report the discovery of a new $z = 7.60$ Ly α detection as well as provide an updated observation of the previously confirmed $z = 7.51$ Ly α emission from Finkelstein et al. (2013) with a $\sim 3\times$ longer exposure time. Our analysis of these Ly α emission line profiles reveal a significant asymmetric shape. The two detected Ly α emission lines from bright sources ($M_{\text{UV}} < -20.25$) could imply that these bright galaxies inhabit ionized bubbles in a partially neutral IGM, although deeper exposures may yet reveal Ly α emission in the fainter sources.

Keywords: early universe — galaxies: distances and redshifts — galaxies: evolution — galaxies: formation — galaxies: high-redshift — intergalactic medium

1. INTRODUCTION

Charting the timeline of reionization through useful tracers such as Ly α forest absorption in high- z quasars (e.g., Becker et al. 2001; Fan et al. 2006; Bolton et al. 2011; Mortlock et al. 2011; McGreer et al. 2015; Bosman et al. 2018), the cosmic microwave background (CMB) polarization mea-

surement (Larson et al. 2011; Planck Collaboration et al. 2016) and Ly α emitter (LAE) observations (e.g., Miralda-Escudé & Rees 1998; Rhoads & Malhotra 2001; Malhotra & Rhoads 2004), constrains how galaxies and the intergalactic medium (IGM) interplay in the early universe. As the dominant sources of the ionizing photons are thought to be galaxies (e.g., Finkelstein et al. 2015; Robertson et al. 2015), investigating the evolution of the IGM during reionization provides critical constraints on the evolution of distant galax-

ies in the early universe as well as the impact of the IGM on the formation and evolution of galaxies at that epoch.

Ly α emission has emerged as a useful tracer of the evolution of the IGM near the end of reionization (e.g., Becker et al. 2018), as Ly α emission is easily diminished with even small amount of neutral hydrogen due to the resonant nature of Ly α scattering with neutral hydrogen (e.g., Rybicki & Loeb 1999; Santos 2004; Dijkstra 2014). For instance, narrow-band Ly α surveys provide a statistical number of Lyman-alpha emitters (LAEs) for Ly α luminosity functions (LFs), and the evolution of the Ly α LF at $z \gtrsim 6$ suggests an increasing fraction of neutral hydrogen in the IGM (e.g., Ouchi et al. 2010; Hu et al. 2010; Kashikawa et al. 2011; Zheng et al. 2017; Konno et al. 2018). From follow-up spectroscopic observations for high- z candidate galaxies or Lyman-break galaxies (LBGs) a simple measure of the Ly α fraction, which is the number of Ly α emitters among the number of spectroscopically observed candidates, shows an apparent deficit of Ly α emission at $z > 6.5$. The drop in Ly α emission at $z > 6$ implies that the HI fraction in the IGM increases significantly from $z \sim 6 \rightarrow 7$ (e.g., Stark et al. 2010; Fontana et al. 2010; Pentericci et al. 2011, 2014; Curtis-Lake et al. 2012; Mallery et al. 2012; Caruana et al. 2012, 2014; Ono et al. 2012; Schenker et al. 2012, 2014; Treu et al. 2012, 2013; Tilvi et al. 2014; Vanzella et al. 2014; Schmidt et al. 2016).

Recently, with extensive Ly α spectroscopic data of $\gtrsim 60$ Ly α detected galaxies at $z \sim 6 - 7$, Pentericci et al. (2018) suggests a smoother evolution of the IGM with their measurement of the Ly α fraction at $z \sim 6 - 7$, where they find little evolution from $z \sim 5 \rightarrow 6$ and a larger drop from $z \sim 6 \rightarrow 7$. This reveals that the IGM was not fully ionized by $z = 6$, thus a smaller evolution in the neutral fraction from $z = 6$ to 7 is needed to explain the observations. An analogous analysis of the Ly α fraction becomes very challenging at $z > 7$. Although spectroscopic follow-up observations with ground-based telescopes and the *Hubble Space Telescope* (HST) grism have been successful in searching for Ly α emission at $z \sim 7$ (e.g., Fontana et al. 2010; Shibuya et al. 2012; Pentericci et al. 2014; Larson et al. 2018), only six Ly α emitting galaxies have been detected so far at $z > 7.5$ (Finkelstein et al. 2013; Oesch et al. 2015; Zitrin et al. 2015; Song et al. 2016; Laporte et al. 2017; Hoag et al. 2018). These non-detections may imply a further drop in the IGM neutral fraction, but this interpretation is non-trivial given the limited spectroscopic depths of most previous NIR spectroscopic observations, and the uncertainty in the expected line wavelength due to the uncertainty of photometric redshift measurements.

In our first paper in this series (Jung et al. 2018) from our *Texas Spectroscopic Search for Ly α Emission at the End of Reionization*, we introduced our methodology for constrain-

ing the evolution of the Ly α EW distribution accounting for all observational incompleteness effects (e.g., photometric redshift probability distribution function, UV continuum luminosity, instrumental wavelength coverage, and observing depth). We found evidence that the Ly α EW distribution evolves to lower values at $z > 6$, suggesting an increasing neutral hydrogen fraction in the IGM. To move to $z > 7$ we require NIR spectroscopy.

We obtained deep NIR spectroscopic data with Keck/MOSFIRE over 84 candidate galaxies. Because these observations partially overlapped on the sky, we achieved $\gtrsim 16$ hr integration time for four high- z candidate galaxies at $z \gtrsim 7$. In this paper, we present the results from these ultra-deep NIR spectroscopic observations with MOSFIRE for four $z \gtrsim 7$ galaxies, reporting a new Ly α emission line at $z = 7.60$ as well as the updated measurement of the previously reported $z = 7.51$ Ly α emitter (Finkelstein et al. 2013) with a $\sim 3\times$ longer exposure time. We describe our MOSFIRE dataset and data reduction procedures in Section 2, and report the detected Ly α emission lines at $z > 7$ in Section 3. Section 4 summarizes our findings with our deepest NIR observations and discusses the Ly α visibility. In this work, we assume the *Planck* cosmology (Planck Collaboration et al. 2016) with $H_0 = 67.8 \text{ km s}^{-1} \text{ Mpc}^{-1}$, $\Omega_M = 0.308$ and $\Omega_\Lambda = 0.692$. The *Hubble Space Telescope* (HST) F435W, F606W, F775W, F814W, F850LP, F105W, F125W, F140W and F160W bands are referred as B_{435} , V_{606} , i_{775} , I_{814} , z_{850} , Y_{105} , J_{125} , JH_{140} and H_{160} , respectively. All magnitudes are given in the AB system (Oke & Gunn 1983), and all errors presented in this paper represent 1σ uncertainties (or central 68% confidence ranges), unless stated otherwise.

2. DATA

2.1. Texas Spectroscopic Search for Ly α Emission at the End of Reionization

To search for Ly α emission from galaxies in the reionization era, we performed deep spectroscopic observations of candidate galaxies in the GOODS-S and GOODS-N fields from the Cosmic Assembly Near-infrared Deep Extragalactic Legacy Survey (CANDELS; PI's Faber & Ferguson). This consists of a total of 18 nights of spectroscopic observations targeting 183 galaxies at $z > 5$: for 118 galaxies with Keck/DEIMOS (PI: R. Livermore) and 84 galaxies with Keck/MOSFIRE (PI: S. Finkelstein; the majority coming through the NASA/Keck allocation). The entire program is described in Jung et al. (2018) where we discuss our measure of the Ly α EW distribution at $z \sim 6.5$ with DEIMOS. The target galaxies were selected from the Finkelstein et al. (2015) photometric catalog. The selection criteria for our masks prioritizes galaxy brightness and the photometric redshift probability being within the Y -band instrumental wavelength coverage to maximize the chance of detecting Ly α

Table 1. Summary of Keck/MOSFIRE observations in GOODS-N

| Mask Name | R.A. (J2000.0) | Decl. (J2000.0) | Observation Dates | N_{targets} | t_{exp} (hrs) | Seeing ^a (arcsec) | Standard Star ^b |
|-----------------|-------------------|--------------------|-----------------------|----------------------|---------------------------|---------------------------------|----------------------------|
| GOODSN_Mask1 | 189.162917 | 62.274244 | 2013 Apr18 | 24 | 5.8 | 0.7 | HIP56147 |
| GOODSN_Mask2 | 189.312875 | 62.279597 | 2013 Apr19 | 19 | 5.5 | 0.6 | HIP56147 |
| GOODSN_Y_v12 | 189.244875 | 62.274253 | 2014 Mar14, 15, 25 | 23 | 6.3 | 0.9 | HIP53735, HIP65280 |
| gdn1404_Y1_3 | 189.339667 | 62.324689 | 2014 Apr17, 18, May13 | 13 | 7.2 | 1.3 | HIP65280 |
| Mask2_Y_2015A | 189.214083 | 62.265297 | 2015 Feb 23, 24 | 10 | 4.5 | 0.8 | HIP56147 |
| Mask1_Y_2015A_2 | 189.331125 | 62.204139 | 2015 Feb 23, 24 | 10 | 4.5 | 1.2 | HIP56147 |

^aFull width at half maximum measured from continuum objects in mask configurations.

^bThe flux calibration standard stars in our long-slit observations, listed in the Hipparcos index (van Leeuwen 2007).

Table 2. Summary of four targets with $t_{\text{exp}} > 16$ hours

| ID ^a | R.A. (J2000.0) | Decl. (J2000.0) | t_{exp} (hrs) | M_{UV}^{b} | z_{phot} | $z_{\text{spec}}^{\text{c}}$ | EW _{Lyα} ^d (\AA) |
|---------------------------|-------------------|--------------------|---------------------------|----------------------------|------------------------|------------------------------|--|
| z7_GND_18869 | 189.205292 | 62.250767 | 16.5 | -19.63 | $7.08^{+0.18}_{-0.16}$ | - | <103.07 |
| z7_GND_16863 | 189.333083 | 62.257236 | 16.3 | -21.24 | $7.23^{+0.28}_{-0.29}$ | 7.60 | 61.28 ± 5.85 |
| z7_GND_42912 ^e | 189.157875 | 62.302372 | 16.5 | -21.58 | $7.54^{+0.19}_{-0.18}$ | 7.51 | 33.19 ± 3.20 |
| z8_GND_9408 | 189.300125 | 62.280358 | 19.0 | -18.99 | $7.71^{+0.47}_{-6.19}$ | - | <386.61 |

^aThe listed IDs are from Finkelstein et al. (2015), encoded with their photometric redshifts and the fields in the CANDELS imaging data.

^b M_{UV} is the averaged magnitude at 1500 \AA , derived from galaxy SED fitting with stellar population synthesis models.

^cThe z_{spec} measurement errors are $\lesssim 0.001$.

^d 5σ upper limits for non-detections.

^eKnown as z8_GND_5296 in Finkelstein et al. (2013).

emission. In this paper we report a new Ly α emission line at $z = 7.60$, analyzing our deepest MOSFIRE observations for four $z \gtrsim 7$ galaxies. The Ly α EW distribution analysis using our entire MOSFIRE dataset will be discussed in our future publication.

2.2. MOSFIRE Y-band observations in GOODS-N

Our GOODS-N MOSFIRE dataset was obtained through 10 nights of observations with six different mask designs from April 2013 to February 2015, targeting 72 galaxies at $z \gtrsim 6$. Table 1 summarizes our Keck/MOSFIRE observations in GOODS-N. In this paper we present the results from our deepest MOSFIRE dataset for the four candidate galaxies, which are summarized in Table 2. We used the Y-band filter with a $0''.7$ slit width and a spectral resolution of $\sim 3\text{\AA}$ ($R = 3500$), covering Ly α over a redshift range of $7.0 < z < 8.2$. In our observations, we take 180 sec exposures in individual frames with an ABAB dither pattern ($+1''.25, -1''.25, +1''.25, -1''.25$), thus the positions in the adjacent frames are separated by $2''.5$.

We note that our GOODS-N MOSFIRE program included six objects with $>16\text{hr}$ integration time, which were classified as high- z candidates from Finkelstein et al. (2015). However, two of the six candidates now appear to more likely be low- z galaxies from an updated photometric redshift measurement including deep I_{814} and *Spitzer*/IRAC photometry (Finkelstein et al. 2019, in prep), which were not included in the Finkelstein et al. (2015) measurement. We note these two likely low- z galaxies show no significant features in their spectra. We thus focus this paper on the remaining four targets. Each of the four targets were observed in three of the MOSFIRE masks, resulting in the longest NIR spectroscopic follow-up observation for Ly α at $z \gtrsim 7$, with a total exposure of $>16\text{hr}$.

2.3. Data Reduction

The data were reduced using Version 2018 of the public MOSFIRE data reduction pipeline (DRP)¹, which provides

¹ <http://keck-datareductionpipelines.github.io/MosfireDRP/>

a sky-subtracted, flat-fielded, and rectified two-dimensional (2D) slit spectrum per object with a wavelength solution using telluric sky emission lines. The reduced 2D spectra have a spectral resolution of $1.09\text{\AA pixel}^{-1}$ and a spatial resolution of $0''.18\text{ pixel}^{-1}$. However, pre-2017 MOSFIRE observations were subject to a noticeable drift of object spectra in the spatial direction along the slit, thought to be due to differential atmospheric refraction (e.g., Kriek et al. 2015; Song et al. 2016). We detected systematic slit drifts (up to $\sim 1\text{ pixel hr}^{-1}$) in all observations, with a noticeable dependence on airmass. To correct for this drifting of object spectra, we ran the MOSFIRE DRP on each adjacent pair of images, and measured the relative slit drift by marking the position of the spectrum of a star we put on one of our slits. Correcting for the derived slit drifts, we combined individual DRP outputs to generate all combined 2D spectra. In the combination step, we rejected any bad pixel or cosmic ray by taking sigma-clipped means, and we measured the best-fit Gaussian peak fluxes of the continuum sources as the weight factors of the DRP outputs.

Flux calibration and telluric absorption correction was done on individual nights, using long-slit observations of a spectro-photometric standard star (listed in Table 1) and the model stellar spectrum of Kurucz (1993). The response curve is obtained by dividing the model stellar spectra (scaled to have the known broadband magnitudes of the standard stars) with the observed spectra from the long-slit observations. In the case where each mask was observed on multiple nights, we combined all 2D spectra, which were individually calibrated, to generate a single 2D spectrum per mask design. We validated our calibration using the known Y_{105} magnitudes of continuum objects in the mask configurations (the magnitudes are from the updated photometric catalog of Finkelstein et al. 2019, in prep). As these objects were observed contemporaneously to our science objects, they were observed under identical conditions, compared to the standard stars which may not have been. We therefore used these objects to calculate and apply a residual normalization correction to our flux calibration array, as the ratio of the known Y -band magnitudes of the slit continuum objects to those from the calibrated spectra, typically up to a $\sim 30 - 50\%$ effect.

All four targets with the longest exposure were observed in three different mask configurations. Thus, after combining all individual mask spectra, weighted by median-noise levels, we obtained fully-reduced, all-mask-combined, and flux-calibrated 2D spectra for the targets. To extract one-dimensional (1D) spectra, we performed an optimal extraction (Horne 1986) with a $2''.5$ spatial aperture.

3. RESULTS

We performed a visual inspection on the reduced 2D and 1D spectra, and found a new $\text{Ly}\alpha$ emission line at $z = 7.60$ from z7_GND_16863 (Figure 1a), in addition to the visi-

ble previously reported $\text{Ly}\alpha$ detection at $z = 7.51$ from z7_GND_42912 (Figure 1b; known as z8_GND_5296 in Finkelstein et al. 2013). The other two targets do not have any obvious emission features at the expected slit positions in the 2D spectra. We also ran the automated line search algorithm from Larson et al. (2018) which searches for significant emission features in 1D spectra. Using a threshold of 5σ for this automated search, this algorithm finds only these same two reported lines, both at a S/N of > 10 .

The $\text{Ly}\alpha$ properties for our detected lines are derived from the best-fit asymmetric Gaussian function obtained by running the IDL MPFIT package (Markwardt 2009). The errors of the derived quantities are estimated via Monte-Carlo (MC) simulations by modulating the 1D spectrum with the 1D noise. We perform MC simulations, fitting the asymmetric Gaussian function to the simulated 1D spectra which are fluctuated by a Gaussian random deviate equal to the associated 1D noise, and we take the standard deviations for the derived $\text{Ly}\alpha$ properties from the MC simulation runs.

3.1. z7_GND_16863: a new $\text{Ly}\alpha$ detection at $z = 7.60$

As shown in the top row of Figure 1 (a) z7_GND_16863 is detected only in the NIR *HST* bands (Y_{105} , J_{125} , and H_{160}), and not in the optical bands (B_{435} , V_{606} , i_{775} , I_{814} , and z_{850}), suggesting strong continuum break and is consistent with the expectation of a $z = 7.60$ galaxy. This object has been targeted in three mask configurations as shown in the bottom right panel of Figure 1 (a): GOODS_N_Mask2 (2013 Apr), GOODS_N_Y_v12 (2014 Mar), and Mask2_Y_2015A (2015 Feb) with a total exposure time of $t_{\text{exp}} = 16.3$ hrs. The emission line has been detected at 10450\AA ($z_{\text{spec}} = 7.60$) with a signal-to-noise (S/N) ratio of 10.8. In the 2D spectrum, the strong emission line is shown at the expected slit position with the two negative features shown at $\pm 2''.5$ separations. Interestingly, this spectroscopic redshift deviates from the photometric redshift at the $\sim 1.5\sigma$ level. Larson et al. (2018) report a 2σ deviation of the photometric redshift from their $z = 7.452$ galaxy, and photometric redshifts show a substantially higher fraction of catastrophic outliers ($\Delta z > 0.15$) in $z \sim 6 - 7$ (Pentericci et al. 2018), compared to low- z universe (Dahlen et al. 2013). Along with these recent findings, a statistical number of spectroscopic redshifts is required to precisely calibrate photometric redshifts in high- z universe at $z > 7$.

The strong break between the optical and NIR bands implies that the emission line is either $\text{Ly}\alpha$ (if it is the Lyman-break) or [O II] $\lambda\lambda 3726, 3729$ (the rest-frame 4000\AA /Balmer break). We note that other emission lines (e.g., $\text{H}\beta$ and [O III] $\lambda\lambda 4959, 5007$, or $\text{H}\alpha$ with [N II] $\lambda\lambda 6548, 6584$) are additionally ruled out as the spectral coverage of our observations would allow us to detect multiple lines, and we do not see additional lines in the 1D or 2D spectrum. In the case

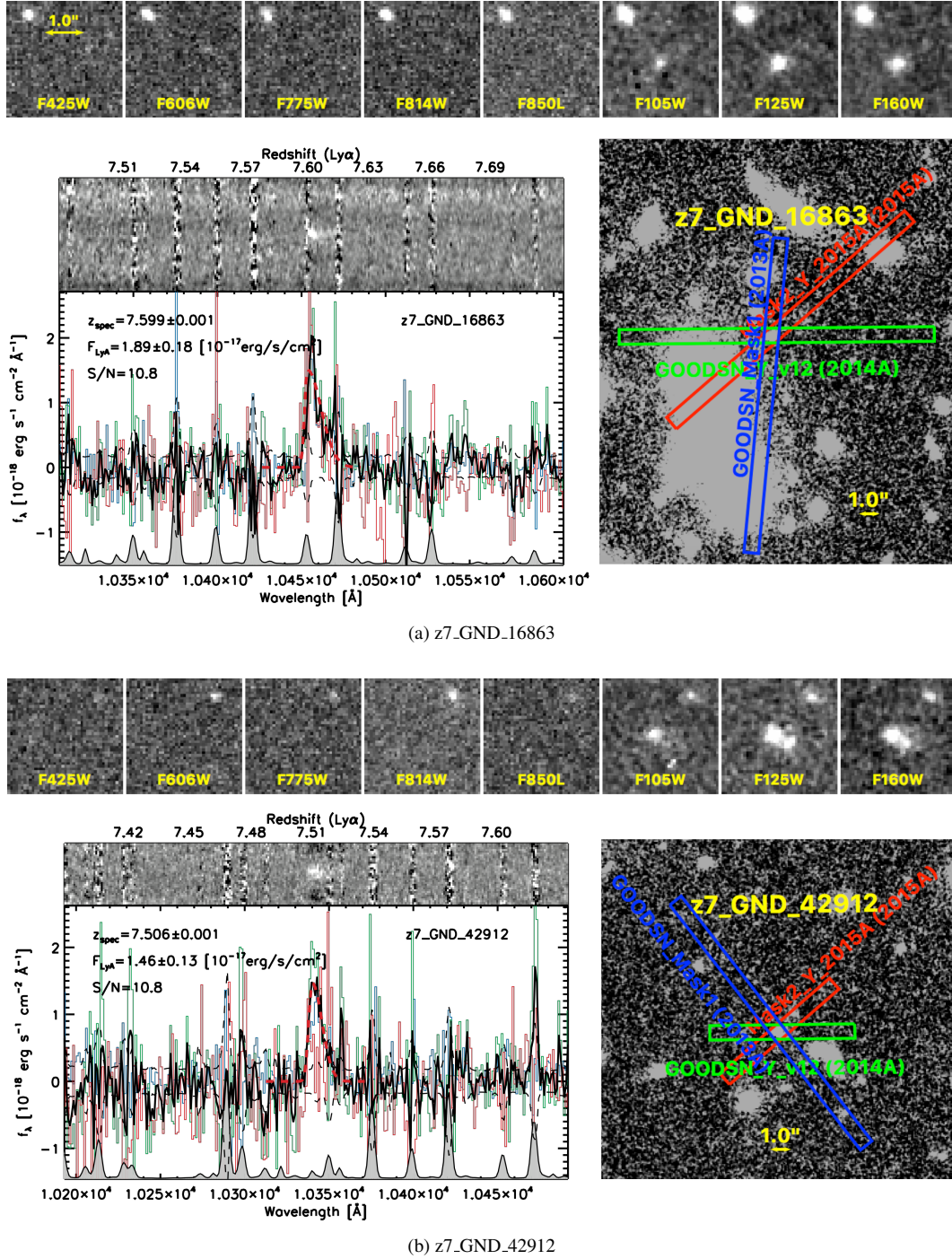


Figure 1. (a) The *HST* ACS/WFC3 images of $z7_GND_16863$ in the top panel. All images are centered on the object, and the Lyman break is clearly observed between the *HST* optical and NIR filters. The bottom left panel shows the 1D and 2D spectra of $z7_GND_16863$. In the 2D spectrum, the strong emission line is shown at the expected spatial slit position with the two negative features shown at $\pm 2''.5$ separation. In the 1D spectrum, the black solid curve is the all-mask-combined flux, and the three individual mask fluxes are displayed as colored histograms. The dashed black curves represent the 1σ noise level, and the normalized sky emission is plotted at the bottom as a grey filled curve. The red dashed curve is the best fit asymmetric Gaussian profile. The bottom right panel shows the slit locations of the three observed mask configurations, overlaid in *HST* WFC3 F160W CANDELS image. The slits are color-coded as histograms in 1D spectra. (b) Same as (a) but for $z7_GND_42912$.

of the [O II] doublet, the MOSFIRE spectral resolution can resolve the doublet with an expected gap of $\sim 8 - 9\text{\AA}$ (at $z = 1.80$, the redshift if this line was [O II]). Thus we analyzed the spectrum for signatures of the other line, with no signal observed at the expected wavelength. Furthermore, double Gaussian line fitting does not satisfy the theoretical expectation on the [O II] doublet flux ratio of $0.35 - 1.5$ (Pradhan et al. 2006). This low- z solution is also disfavored by galaxy SED fitting with a much larger $\chi^2 (= 23.4)$ than that of high- z solution ($\chi^2 = 2.4$) (Figure 2; details described in Section 3.4). Finally, the best fit low- z solution of the object suggests a very dusty but quenched galaxy with a near-zero star formation rate (SFR), inconsistent with strong [O II] emission, which generally implies star formation (although it could also be caused due to active galactic nucleus activity).

Table 3. Summary of Emission Line Properties

| | <i>z7_GND_16863</i> | <i>z7_GND_42912</i> |
|---|-------------------------|------------------------|
| $F_{\text{Ly}\alpha}$ (10^{-17} erg s $^{-1}$ cm $^{-2}$) | 1.89 ± 0.18 | 1.46 ± 0.14 |
| Signal-to-noise Ratio | 10.79 | 10.81 |
| $\text{EW}_{\text{Ly}\alpha}$ (\AA) | 61.28 ± 5.85 | 33.19 ± 3.20 |
| $z_{\text{Ly}\alpha}$ | 7.599 ± 0.001 | 7.506 ± 0.001 |
| σ_{blue} (\AA) | $0.20^{+1.09}_{-0.20}$ | $1.39^{+0.42}_{-0.35}$ |
| σ_{red} (\AA) | $6.25^{+1.29}_{-1.05}$ | $4.11^{+1.00}_{-0.91}$ |
| $\sigma_{\text{red}}/\sigma_{\text{blue}}$ | $> 4.29^a$ | $2.98^{+1.64}_{-1.11}$ |
| FWHM_{red} (\AA) ^b | $14.71^{+3.03}_{-2.46}$ | $9.68^{+2.36}_{-2.15}$ |

^a 1σ lower limit

^b FWHM of the red side of the line ($2.355\sigma_{\text{red}}$)

3.2. *z7_GND_42912*: a Ly α emitter at $z = 7.51$

Our targets also include *z7_GND_42912*, shown in Figure 1(b), which was first reported in Finkelstein et al. (2013) as a new Ly α emission detection at $z = 7.51$ with a S/N ratio of 7.8 from ~ 6 hr of MOSFIRE observations in 2013 April. Here we update the measure of the Ly α line profile from the entire MOSFIRE dataset from three masks: GOODS_N_Mask1 (2013 Apr), GOODS_N_Y_v12 (2014 Mar), and Mask2_Y_2015A (2015 Feb) with $t_{\text{exp}} = 16.5$ hrs (bottom right in Figure 1b). With $\sim 3\times$ longer exposure time, we reveal a clear asymmetric line profile with the updated line flux, $F_{\text{Ly}\alpha} = 1.46 \pm 0.14 \times 10^{-17}$ erg s $^{-1}$ cm $^{-2}$ (S/N = 10.8).

We note that our Ly α flux measurement from *z7_GND_42912* is $\sim 5\times$ greater than that of Finkelstein et al. (2013). Tilvi et al. (2016) published a HST/grism observation of *z7_GND_42912*, finding a ~ 4 times higher Ly α flux than that

of Finkelstein et al. (2013). Although the origin of the significant discrepancy between HST/grism and Keck/MOSFIRE observations was not clearly known by the time, we found that this is mainly due to an unknown flux calibration issue in the Finkelstein et al. (2013) analysis. The c. 2013 version of the MOSFIRE DRP gives different units between the multi-object spectra frames (electrons/sec) and longslit frames (ADU/coadd), but this difference in data units was not documented in the DRP documentation, thus these images were treated in the same manner in Finkelstein et al. (2013). By converting between these two image units, we find that the Finkelstein et al. (2013) line flux should be $4.65\times$ higher, consistent with our updated measurement. Our updated flux with the same dataset (GOODSN_Mask1) is $F_{\text{Ly}\alpha} = 1.28 \pm 0.13 \times 10^{-17}$ erg s $^{-1}$ cm $^{-2}$, now consistent with that of Tilvi et al. (2016). The flux values from the other individual masks are 1.48 and 1.01×10^{-17} erg s $^{-1}$ cm $^{-2}$ with somewhat different line profiles (GOODSN_Y_v12 and Mask2_Y_2015A, respectively). Thus, our final flux value in Table 2, which is measured from all combined data, is higher than the Tilvi et al. (2016) value. We note that while the significant variation in measured line flux between our three observations could imply a systematic uncertainty in our flux calibration, simulations have predicted that the measured Ly α flux can depend on the observed slit position angle due to the complicated morphology of the Ly α emission (Smith et al. 2018).

3.3. Ly α emission properties

The measured emission line properties of the two Ly α emitting galaxies are listed in Table 3. From *z7_GND_16863*, the Ly α emission line has been detected with $F_{\text{Ly}\alpha} = 1.89 \pm 0.18 \times 10^{-17}$ erg s $^{-1}$ cm $^{-2}$ (S/N = 10.8). Although the noise level is very high at the blue side of the line profile due to the nearby sky emission line, the asymmetric feature is still significant, with a 1σ lower limit on $\sigma_{\text{red}}/\sigma_{\text{blue}} > 4.29$. Our new observations of the Ly α emission line from *z7_GND_42912* now reveal a significant asymmetric profile of $\sigma_{\text{red}}/\sigma_{\text{blue}} = 2.98^{+1.64}_{-1.11}$. This significant asymmetry was not found by Finkelstein et al. (2013), but is revealed in our higher fidelity spectrum. We also calculate the skewness of the Ly α emission line profiles, which also suggests significant asymmetry on both emission lines with 1.37 ± 0.23 (*z7_GND_16863*) and 1.69 ± 0.20 (*z7_GND_42912*).

Estimating Ly α asymmetry, Rhoads et al. (2003) introduced the parameters a_f and a_λ which represent the relative flux ratio between blue and red sides of Ly α emission and the relative peak location from the blue and red ends of the line profile. Dawson et al. (2007) performed a statistical study of a_f and a_λ with 59 Ly α emitting galaxies, reporting significant asymmetric Ly α emission profiles at $z \sim 4$. We also estimate a_f and a_λ of our Ly α emission lines with $a_f > 3.70$

and $a_\lambda > 3.43$ for z7_GND.16863 and $a_f > 1.77$ and $a_\lambda > 1.67$ (1σ lower limits), further proving their asymmetry. Furthermore, more recent Ly α surveys investigate Ly α profiles, finding significant asymmetry of Ly α emission lines at $4 < z < 7$ (Ouchi et al. 2010; Hu et al. 2010; Kashikawa et al. 2011; Mallery et al. 2012; U et al. 2015). However, not many high- z Ly α emission lines have reported a significant asymmetric Ly α line profile at $z > 7$, presumably due to low signal-to-noise, though we note the stacked analysis of Ly α emission shows a clear asymmetric line profile in Pentericci et al. (2018). In addition to Song et al. (2016), which captured the first notable asymmetric line profile with deep NIR spectroscopy with 10 hrs of integration time, our analysis of Ly α line profile with the extremely deep spectroscopy uncovers the asymmetric nature of our two Ly α emission lines at $z > 7$.

The asymmetric feature of Ly α emission from high- z galaxies is theoretically expected due to absorption by the interstellar medium (ISM) and IGM. Interaction with an outflowing ISM provides easier escape routes for the red wing of Ly α (e.g., Ahn et al. 2001; Dijkstra 2014), thus the redshifted asymmetric Ly α emission line profile is often explained by common galactic outflows (e.g., Verhamme et al. 2006; Gronke et al. 2015; Remolina-Gutiérrez & Forero-Romero 2019), which could be boosted by cosmic ray (Gronke et al. 2018) and Ly α feedback (Smith et al. 2017; Kimm et al. 2018). Importantly, recent studies on Ly α profiles with Green Peas, a local analogue of a high- z LAEs, have revealed more complex processes related to their Ly α profiles (e.g., Yang et al. 2016, 2017a,b; Verhamme et al. 2018; Orlitová et al. 2018). Therefore, further studies on Ly α profiles are yet required to illustrate the detailed Ly α radiative processes in ISM.

To place Ly α detection limits for our non-detections, we calculate 5σ detection limits of Ly α emission lines in the MOSFIRE Y-band wavelength coverage from $\sim 9800 - 11200\text{\AA}$ by adding mock 1D Ly α emission lines on the actual 1D spectra. For simulating the mock Ly α emission lines, we renormalize the best fit asymmetric Gaussian profile from the detected Ly α emission in z7_GND.42912. The measured median 5σ detection limit of Ly α emission is down to $\sim 4 \times 10^{-18} \text{ erg s}^{-1} \text{ cm}^{-2}$ between sky lines. This measurement is consistent with the previous observations (e.g., Wirth et al. 2015; Song et al. 2016) when scaling our detection limit by \sqrt{t} , where t is the integration time. Compared to the emission line sensitivity in the MOSDEF survey (Kriek et al. 2015), our Ly α sensitivity is lower by up to a factor of two (for an optimistic case of MOSDEF). The difference is understandable as MOSDEF has overall better seeing than our data, and the Ly α line profile is generally broader than other emission lines, making it more difficult to detect.

We measure the rest-frame EWs of the detected Ly α lines and place 5σ EW upper limits for non-detections. The rest-frame EW is defined as the ratio of the Ly α flux to the UV continuum flux density, divided by $1 + z$. We derive the UV continuum brightness from the best-fit galaxy spectral energy distribution (SED) model (refer to Section 3.4), averaged over the 50\AA window just redward of Ly α emission, from $1230\text{\AA} - 1280\text{\AA}$. The derived EWs are $61.28 \pm 5.85\text{\AA}$ and $33.19 \pm 3.20\text{\AA}$ for z7_GND.16863 and z7_GND.42912, respectively. Previous measures of Ly α EWs in the literature show a deficit of high EW LAEs ($>50\text{\AA}$) at $z > 7$ (e.g., Tilvi et al. 2014, and references therein), and the measured EW of the Ly α emission line from z7_GND.42912 ($33.19 \pm 3.20\text{\AA}$) is consistent with those measurements. However, the Ly α EW from the new Ly α emission line in z7_GND.16863 ($61.28 \pm 5.85\text{\AA}$) is relatively high. Along with the recent observations of Hu et al. (2017), Zheng et al. (2017), and Pentericci et al. (2018) which found high EW LAEs at $z \sim 7$ and Larson et al. (2018) which reported a high EW object ($140.3 \pm 19.0\text{\AA}$) at $z \sim 7.5$, our results show that high-EW Ly α emission is not uncommon at $z > 7$.

Even with our very deep NIR observations, we do not detect Ly α emission from z7_GND.18869 and z7_GND.9408. However, those are faint objects, having large EW upper limits (<103 and $<387 \text{\AA}$, respectively), thus non-detections from the two faint galaxies are well expected and understandable. However, detecting Ly α lines from two out of two observed bright sources is somewhat unexpected, due to previous results implying an increasing neutral fraction of the IGM at $z > 7$.

The MOSFIRE Y-band covers the wavelength ranges of N V emission lines, an indicator of active galactic nuclei (AGN) activity, for our two LAEs. For z7_GND.16863, we search within 500 km s^{-1} from the expected wavelength (e.g., Steidel et al. 2010; Erb et al. 2014; Stark et al. 2017; Mainali et al. 2018), finding no significant detection, and a 1σ upper limit on the N V emission line flux of $\lesssim 8.54 \times 10^{-19} \text{ erg s}^{-1} \text{ cm}^{-2}$, corresponding to the Ly α / N V flux ratio $\gtrsim 22$. For z7_GND.42912, Hutchison et al. (2019, in prep) detect one of the C III] lines with MOSFIRE H-band observations, measuring the systematic redshift to be $z = 7.5027 \pm 0.0003$ and 7.4941 ± 0.0003 , if their detected line is C III] $\lambda 1907$ and C III] $\lambda 1909$, respectively. We do not see significant emission for N V at the wavelengths corresponding to these systemic redshifts, and we measure 1σ upper limits of <7.66 and $<6.60 \times 10^{-19} \text{ erg s}^{-1} \text{ cm}^{-2}$ at 10543 and 10532\AA , corresponding to Ly α / N V flux ratios of >19 and >22 , respectively. Tilvi et al. (2016) measured a possible detection of N V from z7_GND.42912 at $\lambda \sim 10550\text{\AA}$ with a slight spatial offset of ~ 0.1 from HST/grism observations, with a reported N V line flux of $f_{\text{line}} = 0.91 \pm 0.21 \times 10^{-17} \text{ erg s}^{-1} \text{ cm}^{-2}$. Our spectrum should have detected this line with S/N

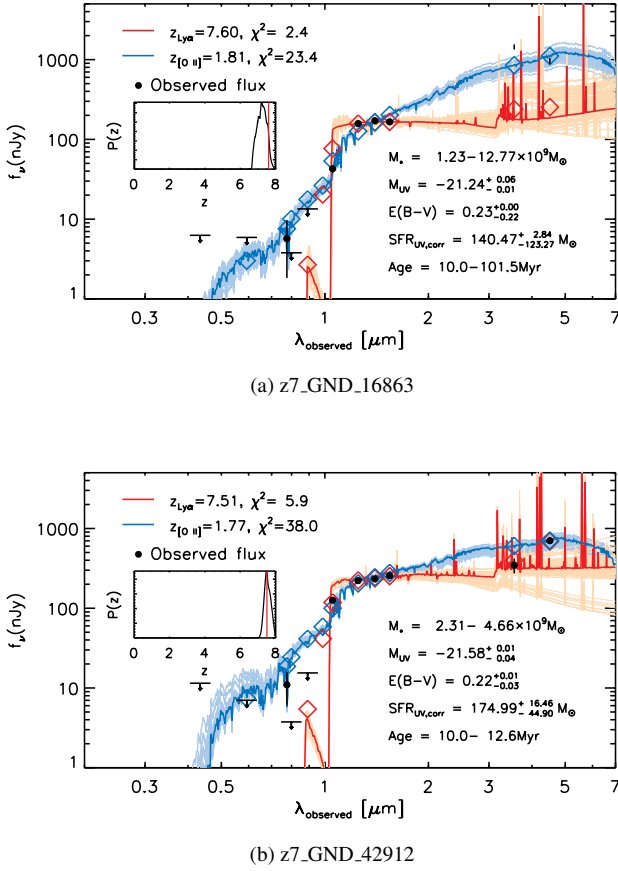


Figure 2. Galaxy SED fitting results. Each panel shows two SEDs for high- z ($\text{Ly}\alpha$) and low- z ([O II]) solutions (red and blue solid curves, respectively), and colored diamond symbols represent continuum fluxes from the model SEDs. Black dots are observed fluxes with their associated errors, and the downward arrows are 1σ upper limits. The physical quantities written in the panels are estimated from the high- z solutions. For stellar masses and ages, we display 68% confidence ranges. Insets display photometric redshift probability distributions, $P(z)$, taken from Finkelstein et al. (2019, in prep), and the spectroscopic redshifts are shown with vertical red lines.

> 10 . This our non-detection implies that the previously reported N V in Tilvi et al. (2016) may be contamination. The previously reported measures of the $\text{Ly}\alpha / \text{N V}$ flux ratio from several $z \gtrsim 7$ galaxies range from $\sim 1 - 2$ (Hu et al. 2017; Sobral et al. 2017) to $\sim 6 - 9$ (Laporte et al. 2017; Mainali et al. 2018). With the limits of the $\text{Ly}\alpha / \text{N V}$ flux ratio $\gtrsim 19 - 22$ in our observations, our two LAEs likely do not host significant AGN activity (see also discussion in Castellano et al. 2018).

3.4. Physical Properties of $z \sim 7.5$ Galaxies

To derive the physical quantities of our detected galaxies, we perform galaxy spectral energy distribution (SED) fitting

with stellar population synthesis models (Bruzual & Charlot 2003). The parameter settings, nebular emission lines (Inoue 2011; Salmon et al. 2015), and IGM attenuation (Madau 1995) descriptions in SED fitting are similar to those used in Jung et al. (2017). We take a Salpeter (1955) initial mass function with lower and upper stellar-mass limits of 0.1 to $100 M_{\odot}$, respectively, and metallicities range from 0.005 to $1.0 Z_{\odot}$. We allow several star-formation histories (SFHs), using a range of exponential models: decrease, increase, and constant SFHs with exponential-decaying time ($\tau = 10\text{Myr}, 100\text{Myr}, 1\text{Gyr}, 10\text{Gyr}, 100\text{Gyr}, -300\text{Gyr}, -1\text{Gyr}, -10\text{Gyr}$). Dust attenuation to our model spectra uses the attenuation curve of Calzetti (2001) with $E(B - V)$ values spanning $0 - 0.8$. We restrict stellar population ages to be > 10 Myr, to avoid a scenario where a galaxy forms all of its mass in an unphysically small amount of time.

Constraining the stellar mass for high- z galaxies is critically dependent on long wavelength *Spitzer*/IRAC photometry. However, z7_GND_16863 is found in the vicinity of a bright nearby source (Figure 1a), making it impossible to properly measure its rest-frame optical continuum with the low spatial resolution IRAC photometry. Thus, our SED fitting results of z7_GND_16863 with only rest-frame UV fluxes have highly correlated physical parameters (e.g., stellar mass, dust extinction, and age). The $\text{Ly}\alpha$ contributions to continuum fluxes were removed during the SED fitting, and we also ignored Y_{105} fluxes as it is often difficult to model due to the uncertainty of IGM attenuation. To calculate SFRs, we first obtained dust-corrected UV fluxes from the best fit models and convert the UV fluxes to SFRs by adopting the updated FUV-to-SFR conversion factor of $\kappa = 1.15 \times 10^{-28} M_{\odot} \text{yr}^{-1} \text{erg}^{-1} \text{s Hz}$ (Madau & Dickinson 2014). This is derived from the stellar population models of Conroy et al. (2009) and $\sim 20\%$ lower than the conventional conversion factor in Kennicutt (1998). This is also similar to the other recent studies (e.g., Salim et al. 2007; Haardt & Madau 2012) based on Bruzual & Charlot (2003) which found lower mean conversion factors.

Figure 2 shows our SED fitting results for z7_GND_16863 (top) and z7_GND_42912 (bottom). The best fit model is chosen by minimizing χ^2 . The fitting errors are obtained via Monte-Carlo (MC) simulations. We run 1000 MC simulations to derive the best fit models with the simulated continuum fluxes. In the MC simulations, we fluctuate the observed fluxes with Gaussian random deviates which is equivalent to the flux measurement errors to simulate the continuum fluxes, and we perform SED fitting with the simulated fluxes.

z7_GND_16863 and z7_GND_42912 are very bright in the rest-frame UV ($M_{\text{UV}} = -21.24$ and -21.58 , respectively), relative to the characteristic UV magnitudes of $z \sim 7 - 8$ galaxies of $M_{\text{UV}} \sim 21$ (Finkelstein et al. 2015). Stel-

lar masses of the two objects are consistent with that expected from published scaling relation between $M_* - M_{UV}$ at $z > 7$ (Song et al. 2016), although the stellar mass of z7_GND_16863 is not well-constrained due to the lack of the rest-frame optical photometric constraints. The two Ly α emitters are actively forming stars with SFRs [$M_\odot \text{ yr}^{-1}$] = 140_{-123}^{+3} (z7_GND_16863) and 175_{-45}^{+16} (z7_GND_42912). These SFRs are above the fiducial $M_* - \text{SFR}$ relation of high- z galaxies (e.g., Salmon et al. 2015; Song et al. 2016; Jung et al. 2017) which suggests $\sim 10 - 30 M_\odot \text{ yr}^{-1}$ for $\sim 10^{9-10} M_\odot$ galaxies at $z \sim 6$, although this relation likely increases at higher redshift. Particularly, our updated measurement of z7_GND_42912 with young stellar populations (age < 12.6 Myr) and a high SFR is yet comparable but less extreme than Finkelstein et al. (2013), which found the time-averaged SFR of z7_GND_42912 higher than $330 M_\odot \text{ yr}^{-1}$ with extremely young stellar populations (age $\sim 1-3$ Myr [1σ], which is less than we allowed in our model fitting). We also calculate time averaged SFRs by simply dividing the stellar mass by the stellar population age. The averaged SFRs of the galaxies are $\gtrsim 85$ and $\gtrsim 216 M_\odot \text{ yr}^{-1}$ in their 1σ low limits for z7_GND_16863 and z7_GND_42912, respectively. Even with their large uncertainties, our $z \sim 7.5$ Ly α emitting galaxies require high SFRs to build up their stellar masses. Such high SFRs are expected for producing their asymmetric Ly α profiles with strong galactic outflows due to stellar feedback.

4. SUMMARY AND DISCUSSION

We analyze our deepest NIR spectroscopic observations with Keck/MOSFIRE for four target galaxies at $z_{\text{phot}} \gtrsim 7$ with $\gtrsim 16$ hr of integration time. We detect two Ly α emission lines from UV-bright and actively star-forming galaxies, discovering a new Ly α emitting system at $z = 7.60$ (z7_GND_16863) as well as providing an updated measure of a $z = 7.51$ Ly α emission line (z7_GND_42912) which was previously reported in Finkelstein et al. (2013) and Tilvi et al. (2016). We measure the detailed Ly α line profiles, finding significant Ly α asymmetry. The two detected Ly α emission lines from bright sources ($M_{UV} < -20.25$) could imply that these bright galaxies likely inhabit ionized bubbles in a partially neutral IGM, although deeper exposures may yet reveal Ly α emission in the fainter sources.

With the current consensus from Ly α studies around the end of reionization at $z \sim 6 - 7$, Ly α visibility is expected to decrease as the IGM becomes neutral into the epoch of reionization, and it is also expected to have a significant dependence on the UV brightness of galaxies. Conventionally, galaxies are divided into bright ($M_{UV} < -20.25$) and faint ($M_{UV} > -20.25$) groups, and the Ly α fraction is observationally suggested to be higher from faint sources than that from bright ones (e.g., Stark 2016, and references therein).

Particularly, Pentericci et al. (2018) found a higher Ly α fraction among faint samples again at $z \sim 7$. This is explained by bright galaxies being more likely to be evolved, with a higher metallicity and larger amount of dust, reducing the Ly α photon escape probability.

On the contrary, previous results at $z > 7$ (Stark et al. 2017) suggest that very bright galaxies reside in ionized bubbles, allowing a larger transmission of Ly α emission than faint sources. Similarly, Castellano et al. (2018) found more Ly α detections than expected among bright galaxies, while they failed to find faint galaxies which emit Ly α photons at $z \sim 7$. A possible explanation is that brighter galaxies reside in early overdensities, which are ionized earlier compared to the rest of the Universe. In addition, as discussed in Mason et al. (2018), Ly α photons from bright sources could escape easier due to their higher velocity offsets from systemic, making them less affected by neutral hydrogen in the IGM.

Furthermore, Zheng et al. (2017) reports a "bump" at the bright end of the Ly α LF at $z \sim 7$ from the Lyman Alpha Galaxies in the Epoch of Reionization (LAGER) survey, indicative of large ionized bubbles where we could see different evolution at bright and faint ends of the Ly α LF. In the same context, our two detected Ly α emission lines from bright sources are suggestive that the Ly α visibility of UV-bright galaxies does not decrease as much as that of faint galaxies at $z > 7$. Of course, this is highly tentative as the number of targets in our study is small, and the Ly α EW detection limits for our faint sources are not as deep as those for the bright ones. Therefore, a comprehensive analysis is necessary to assure if the Ly α detection rate is higher among brighter galaxies at $z > 7$.

Our entire MOSFIRE dataset will be included in the next publication where we will place a strong constraint on the Ly α visibility into $z > 7$ with the most comprehensive dataset of NIR spectroscopic follow-up observations. Furthermore, Ly α studies in the even earlier universe is promising with the *James Webb Space Telescope* NIR spectroscopy (Smith et al. 2018), and a future Ly α survey project with the extremely large telescopes (e.g., the Giant Magellan Telescope) will deliver an extensive Ly α dataset, which allows us to explore large areas and study the topology of reionization.

The authors wish to acknowledge the very significant cultural role and reverence that the summit of Mauna Kea has always had within the indigenous Hawaiian community. We are most fortunate to have the opportunity to conduct our observations from this mountain. I.J. acknowledges support from the NASA Headquarters under the NASA Earth and Space Science Fellowship Program - Grant 80NSSC17K0532. I.J. and S.F. acknowledge support from NSF AAG award AST-1518183.

REFERENCES

- Ahn, S.-H., Lee, H.-W., & Lee, H. M. 2001, *ApJ*, 554, 604
- Becker, R. H., Fan, X., White, R. L., et al. 2001, *AJ*, 122, 2850
- Becker, G. D., Davies, F. B., Furlanetto, S. R., et al. 2018, *ApJ*, 863, 92
- Bolton, J. S., Haehnelt, M. G., Warren, S. J., et al. 2011, *MNRAS*, 416, L70
- Bosman, S. E. I., Fan, X., Jiang, L., et al. 2018, *MNRAS*, 479, 1055
- Bruzual, G., & Charlot, S. 2003, *MNRAS*, 344, 1000
- Calzetti, D. 2001, *New Astron.*, 45, 601
- Caruana, J., Bunker, A. J., Wilkins, S. M., et al. 2012, *MNRAS*, 427, 3055
- Caruana, J., Bunker, A. J., Wilkins, S. M., et al. 2014, *MNRAS*, 443, 2831
- Castellano, M., Pentericci, L., Vanzella, E., et al. 2018, *ApJL*, 863, L3
- Conroy, C., Gunn, J. E., & White, M. 2009, *ApJ*, 699, 486
- Curtis-Lake, E., McLure, R. J., Pearce, H. J., et al. 2012, *MNRAS*, 422, 1425
- Dahlen, T., Mobasher, B., Faber, S. M., et al. 2013, *ApJ*, 775, 93
- Dawson, S., Rhoads, J. E., Malhotra, S., et al. 2007, *ApJ*, 671, 1227
- Dijkstra, M. 2014, *PASA*, 31, e040
- Erb, D. K., Steidel, C. C., Trainor, R. F., et al. 2014, *ApJ*, 795, 33
- Fan, X., Strauss, M. A., Becker, R. H., et al. 2006, *AJ*, 132, 117
- Finkelstein, S. L., Papovich, C., Dickinson, M., et al. 2013, *Nature*, 502, 524
- Finkelstein, S. L., Ryan, R. E., Jr., Papovich, C., et al. 2015, *ApJ*, 810, 71
- Fontana, A., Vanzella, E., Pentericci, L., et al. 2010, *ApJL*, 725, L205
- Gronke, M., Bull, P., & Dijkstra, M. 2015, *ApJ*, 812, 123
- Gronke, M., Girichidis, P., Naab, T., & Walch, S. 2018, *ApJL*, 862, L7
- Haardt, F., & Madau, P. 2012, *ApJ*, 746, 125
- Hoag, A., Bradač, M., Brammer, G., et al. 2018, *ApJ*, 854, 39
- Horne, K. 1986, *PASP*, 98, 609
- Hu, E. M., Cowie, L. L., Barger, A. J., et al. 2010, *ApJ*, 725, 394
- Hu, W., Wang, J., Zheng, Z.-Y., et al. 2017, *ApJL*, 845, L16
- Inoue, A. K. 2011, *MNRAS*, 415, 2920
- Jung, I., Finkelstein, S. L., Song, M., et al. 2017, *ApJ*, 834, 81
- Jung, I., Finkelstein, S. L., Livermore, R. C., et al. 2018, *ApJ*, 864, 103
- Kashikawa, N., Shimasaku, K., Matsuda, Y., et al. 2011, *ApJ*, 734, 119
- Kennicutt, R. C., Jr. 1998, *ARA&A*, 36, 189
- Kimm, T., Haehnelt, M., Blaizot, J., et al. 2018, *MNRAS*, 475, 4617
- Konno, A., Ouchi, M., Shibuya, T., et al. 2018, *PASJ*, 70, S16
- Kriek, M., Shapley, A. E., Reddy, N. A., et al. 2015, *ApJS*, 218, 15
- Kurucz, R. L. 1993, *Kurucz CD-ROM*, Cambridge, MA: Smithsonian Astrophysical Observatory, —c1993, December 4, 1993,
- Laporte, N., Ellis, R. S., Boone, F., et al. 2017, *ApJL*, 837, L21
- Larson, D., Dunkley, J., Hinshaw, G., et al. 2011, *ApJS*, 192, 16
- Larson, R. L., Finkelstein, S. L., Pirzkal, N., et al. 2018, *ApJ*, 858, 94
- Madau, P. 1995, *ApJ*, 441, 18
- Mainali, R., Zitrin, A., Stark, D. P., et al. 2018, *MNRAS*, 479, 1180
- Malhotra, S., & Rhoads, J. E. 2004, *ApJL*, 617, L5
- Mallery, R. P., Mobasher, B., Capak, P., et al. 2012, *ApJ*, 760, 128
- Markwardt, C. B. 2009, *Astronomical Data Analysis Software and Systems XVIII*, 411, 251
- Mason, C. A., Treu, T., de Barros, S., et al. 2018, *ApJL*, 857, L11
- McGreer, I. D., Mesinger, A., & D’Odorico, V. 2015, *MNRAS*, 447, 499
- Miralda-Escudé, J., & Rees, M. J. 1998, *ApJ*, 497, 21
- Mortlock, D. J., Warren, S. J., Venemans, B. P., et al. 2011, *Nature*, 474, 616
- Oesch, P. A., van Dokkum, P. G., Illingworth, G. D., et al. 2015, *ApJL*, 804, L30
- Oke, J. B., & Gunn, J. E. 1983, *ApJ*, 266, 713
- Ono, Y., Ouchi, M., Mobasher, B., et al. 2012, *ApJ*, 744, 83
- Orlítóvá, I., Verhamme, A., Henry, A., et al. 2018, *A&A*, 616, A60
- Ouchi, M., Shimasaku, K., Furusawa, H., et al. 2010, *ApJ*, 723, 869
- Pentericci, L., Fontana, A., Vanzella, E., et al. 2011, *ApJ*, 743, 132
- Pentericci, L., Vanzella, E., Fontana, A., et al. 2014, *ApJ*, 793, 113
- Pentericci, L., Vanzella, E., Castellano, M., et al. 2018, *A&A*, 619, A147
- Planck Collaboration, Ade, P. A. R., Aghanim, N., et al. 2016, *A&A*, 594, A13
- Pradhan, A. K., Montenegro, M., Nahar, S. N., & Eissner, W. 2006, *MNRAS*, 366, L6
- Remolina-Gutiérrez, M. C., & Forero-Romero, J. E. 2019, *MNRAS*, 482, 4553
- Rhoads, J. E., & Malhotra, S. 2001, *ApJL*, 563, L5
- Rhoads, J. E., Dey, A., Malhotra, S., et al. 2003, *AJ*, 125, 1006
- Robertson, B. E., Ellis, R. S., Furlanetto, S. R., & Dunlop, J. S. 2015, *ApJL*, 802, L19
- Rybicki, G. B., & Loeb, A. 1999, *ApJL*, 520, L79
- Salim, S., Rich, R. M., Charlot, S., et al. 2007, *ApJS*, 173, 267
- Salmon, B., Papovich, C., Finkelstein, S. L., et al. 2015, *ApJ*, 799, 183
- Salpeter, E. E. 1955, *ApJ*, 121, 161
- Santos, M. R. 2004, *MNRAS*, 349, 1137
- Schenker, M. A., Ellis, R. S., Konidaris, N. P., & Stark, D. P. 2014, *ApJ*, 795, 20
- Schenker, M. A., Stark, D. P., Ellis, R. S., et al. 2012, *ApJ*, 744, 179
- Schmidt, K. B., Treu, T., Bradač, M., et al. 2016, *ApJ*, 818, 38
- Shibuya, T., Kashikawa, N., Ota, K., et al. 2012, *ApJ*, 752, 114
- Smith, A., Bromm, V., & Loeb, A. 2017, *MNRAS*, 464, 2963
- Smith, A., Ma, X., Bromm, V., et al. 2018, *arXiv:1810.08185*
- Sobral, D., Matthee, J., Best, P., et al. 2017, *MNRAS*, 466, 1242
- Song, M., Finkelstein, S. L., Ashby, M. L. N., et al. 2016, *ApJ*, 825, 5
- Song, M., Finkelstein, S. L., Livermore, R. C., et al. 2016, *ApJ*, 826, 113
- Stark, D. P., Ellis, R. S., Chiu, K., Ouchi, M., & Bunker, A. 2010, *MNRAS*, 408, 1628
- Stark, D. P. 2016, *ARA&A*, 54, 761
- Stark, D. P., Ellis, R. S., Charlot, S., et al. 2017, *MNRAS*, 464, 469
- Steidel, C. C., Erb, D. K., Shapley, A. E., et al. 2010, *ApJ*, 717, 289
- Tilvi, V., Papovich, C., Finkelstein, S. L., et al. 2014, *ApJ*, 794, 5
- Tilvi, V., Pirzkal, N., Malhotra, S., et al. 2016, *ApJL*, 827, L14
- Treu, T., Schmidt, K. B., Trenti, M., Bradley, L. D., & Stiavelli, M. 2013, *ApJL*, 775, L29
- Treu, T., Trenti, M., Stiavelli, M., Auger, M. W., & Bradley, L. D. 2012, *ApJ*, 747, 27
- U, V., Hemmati, S., Darvish, B., et al. 2015, *ApJ*, 815, 57
- van Leeuwen, F. 2007, *A&A*, 474, 653
- Vanzella, E., Fontana, A., Pentericci, L., et al. 2014, *A&A*, 569, A78
- Verhamme, A., Schaerer, D., & Maselli, A. 2006, *A&A*, 460, 397
- Verhamme, A., Garel, T., Ventou, E., et al. 2018, *MNRAS*, 478, L60
- Wirth, G. D., Trump, J. R., Barro, G., et al. 2015, *AJ*, 150, 153
- Yang, H., Malhotra, S., Gronke, M., et al. 2016, *ApJ*, 820, 130
- Yang, H., Malhotra, S., Rhoads, J. E., et al. 2017, *ApJ*, 838, 4
- Yang, H., Malhotra, S., Gronke, M., et al. 2017, *ApJ*, 844, 171
- Zheng, Z.-Y., Wang, J., Rhoads, J., et al. 2017, *ApJL*, 842, L22
- Zitrin, A., Labbé, I., Belli, S., et al. 2015, *ApJL*, 810, L12